Characterization of photonic crystal coupling to and from guided light by absorbance

Lucie Devys, Géraldine Dantelle, Viacheslav Kubytskyi, Henri Benisty, Thierry Gacoin

Characterization of photonic crystal coupling to and from guided light by absorbance

Lucie Devys,[a,*] Géraldine Dantelle,[a] Viacheslav Kubytskyi,[a] Henri Benisty,[b] and Thierry Gacoin[a]

[a]Laboratoire de Physique de la Matière Condensée, UMR CNRS 7643, Ecole Polytechnique, 91128 PALAISEAU Cedex, France

[b]Laboratoire Charles Fabry de l'Institut d'Optique, CNRS, Université Paris-Sud, Campus Polytechnique, RD 128, F-91127 Palaiseau Cedex, France

Abstract. We considered luminescent TiO_2 films whose surface was imprinted with a two-dimensional (2-D) square shaped photonic crystal with different pattern depths (from 20 to 61 nm). The aim of this work is to develop a straightforward method to characterize the PhC efficiency on light extraction. Transmission spectra of the patterned areas as obtained using a routine spectrometer exhibit peaks evidencing the coupling by the photonic crystal structure of free-space light with guided modes within the film, in good agreement with 2-D rigorous-coupled wave analysis (RCWA) simulations. As expected, the deeper the pattern depth, the stronger the coupling between the guided light and the photonic crystal. RCWA simulations allow evaluating quantitatively the extraction length, characteristic of the efficiency of light extraction, from the transmission spectra, in good agreement with direct measurements.

Keywords: extraction length; patterning; photonic crystal; rigorous-coupled wave analysis

1 Introduction

One of the main challenges for light emitting devices [light emitting diodes (LEDs), organic LEDs, plasma displays, etc.] is efficient light extraction. Due to the different refractive indices (especially for those technologies using semiconductors), light emitted in solids undergoes internal reflections and a significant amount of the useful light is thus trapped in the device, limiting the external yield of many systems.[1] Specific strategies must be carried out to extract this light. Two main approaches are described in the literature: the one based on scattering centers[2,3] or surface roughness[4] and the other one using periodic structuration of the surface.[5,6] The choice of periodicity is rather simple for basic periodic structures and nearly single mode waveguides, as the laws of gratings leave little room to transform a guided mode into a mode propagating in air. When looking in finer details with issues such as grating shape, depth, however, things are less simple. Generally speaking, the efficiency of such a structure is determined by the coupling between the guided modes propagating in the device and the radiation modes, which is characterized in the literature by the measurement of light extraction length, corresponding to the length of light propagation in the film before being extracted. In first approximation, it is well known that the stronger the coupling, the shorter the extraction length.

Matioli et al.[7] demonstrated that the extraction length can be deduced from the width of the diffraction peaks observed on 2-D emission maps in the case of GaN-based LEDs. However, for ~100-μm extraction length, such experiment requires a high-resolution angle-spectrum-resolved

*Address all correspondence to: Lucie Devys, E-mail: lucie.devys@polytechnique.edu

set-up. More recently, a straightforward method to determine the extraction length was described by Devys et al.[8] based on the direct observation of the extinction of the guided mode. Nevertheless, all these characterizations require a dedicated optical bench, which needs time to be set up and optimized.

In this article, we present a new and straightforward method to characterize the PhC efficiency on light extraction, based on light transmission measurements in routine spectrometers, as light extraction and light injection are highly correlated. In essence, the process of light injection in a film is indeed the reverse of extraction as illustrated in Fig. 1. For light injection, in the case of an unpatterned sample, whatever the wavelength of a normal incident wave, light is either reflected or transmitted; there is no excitation of the guided mode in the TiO_2 layer. On the contrary, if the sample is structured, there is a resonant wavelength which couples to the guide mode. For light extraction, by introducing an emitting dipole oriented perpendicularly to the layer (i.e., emission in the direction of the guided mode), a guided mode settles in the system. In the case of an unpatterned sample, the light is completely trapped. Quite the reverse, if the sample is structured, the light at a given wavelength is extracted in the air and in the substrate. This resonant wavelength is the same as the one of the light injection case. The graph shows that in the case of the pattering, the intensity of the guided mode is attenuated because of light escaping to the air and the substrate.

We show here that the efficiency of coupling between an incident beam and the patterned system can be easily determined by an absorption measurement in a transmission configuration using a common laboratory UV-vis spectrometer apparatus. An important point for physical understanding is that light is not genuinely absorbed by the film but diverted within the film, causing nevertheless absorbance lines that appear on the absorption spectra,[9,10] as will be exemplified here. For this study, we consider a model system, consisting of a TiO_2 sol-gel layer doped with europium chelates deposited onto a glass substrate and an upper TiO_2 layer, which is structured by nanoimprint lithography.[6]

2 Experimental Section

2.1 *Synthesis of TiO_2 Thin Film*

Thin films of TiO_2 are produced according to the process described in Ref. 6. Europium complexes $Eu(TTA)_3$ are synthesized following the process previously described by De Silva et al.[11]

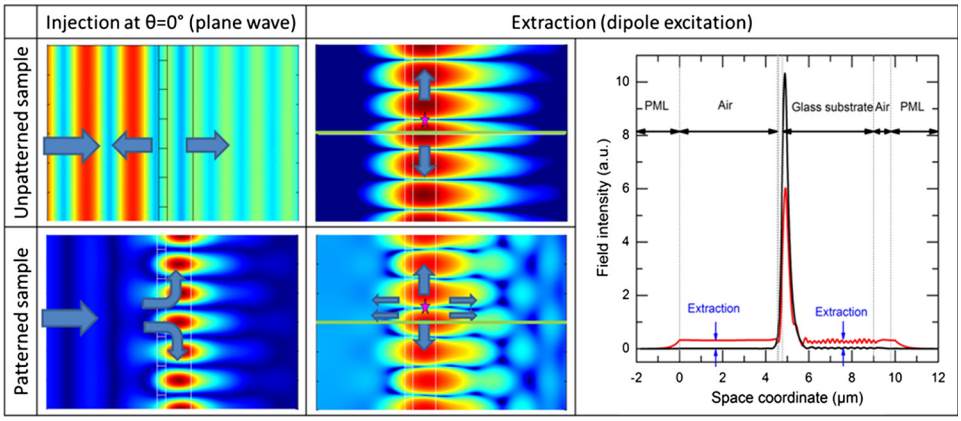

Fig. 1 Similarity between light injection and light extraction mechanisms. The system geometry is explained on the graph. It consists of a TiO_2 layer of 236 nm on top of a glass substrate. In the patterned case, the first 61 nm of the TiO_2 layer at the air interface is structured with a regular square geometry (period 400 nm). PML is a perfectly matched layer, which absorbs outgoing waves without reflection into the computational domain. The colors only reflect the intensity of the field, red corresponding to the highest intensity and blue to the weakest. The pink star represents an emitting dipole. The intensity along the green cut is shown in the graph. The black curve corresponds to the cut of the unpatterned sample, and the red one to the patterned one. Colored figure available online.

This europium chelate is soluble in ethanol, thus it is simply dissolved in the TiO_2 sol with a concentration of 20 mg/mL. Excitation of such chelates occurs in the UV range and main emission is situated at 612 nm.

The sol containing the emitting molecules is deposited by spin-coating (2000 rpm, 30 s) onto glass substrates previously cleaned by an UV-Ozone treatment for 15 min at 50°C (Novascan cleaner, École Polytechnique, France). A thermal treatment (5 min at 110°C) allows the sol condensation. The obtained thin film of amorphous TiO_2 presents an optical index of 1.75 at 612 nm, as measured by ellipsometry.

2.2 *Surface Patterning*

On the top of the luminescent TiO_2 layer is deposited a second TiO_2 layer for surface structuration. This architecture is chosen in order to make sure that the same amount of emitters is present in the whole film despite patterning. This second sol is different from the one used for the thin film containing the light emitters because the condensation of the latter appears too quickly. The solution of TiO_2 molecular precursors is complexed by acetylacetone, which delays the condensation.[12] The obtained sol has a Ti concentration c_{max} of 1.2×10^{-3} mol/L. It is spin-coated (3000 rpm 30 s) onto the film doped with europium chelates. Before complete TiO_2 condensation, a square polydimethylsiloxane (PDMS) mold with 400-nm period is applied onto the film surface. According to Eq. (1) and taking into consideration a 200-nm film with a refractive index of 1.75 presenting a guided mode with an effective index n_{eff} of 1.58, such a mold period a is perfectly appropriate to extract the main emission wavelength of the chelate ($\lambda = 620$ nm) near the sample normal:

$$a = \frac{\lambda}{n_{eff}}. \tag{1}$$

The system is then introduced into an NXR2500 imprinter from Nanonex, where it is heated at 110°C under a pressure of 20 psi for 5 min. The grafting of trimethylchlorosilane (TMCS) on the mold prevents the adhesion between the PDMS and the TiO_2 and facilitates the unmolding after cooling.

The thickness of the upper TiO_2 layer, d, is modified by changing the concentration of Ti precursors in the sol. Three different samples, Films A, B, and C, are prepared using respectively three different concentrations of Ti precursors, $c_{max}/4$, $c_{max}/2$, and c_{max} after dilution in isopropanol (Table 1).

2.3 *Structural Characterizations*

The homogeneity and quality of the films as well as the accuracy between the mold and the pattern imprinted in the TiO_2 were checked by atomic force microscopy (AFM) and scanning electron microscopy (SEM, Hitachi S4800 microscope, École Polytechnique). Moreover for each film the structural characteristics were precisely determined. The thickness of the layer containing the light emitters, e (Fig. 2), was measured by profilometry (Dektak 150 profilometer, École Polytechnique, Palaiseau, France) prior to the deposition of the TiO_2 sublayer. It appeared

Table 1 Structural characteristics of the three films.

	Sol concentration	Film thickness $t + e$ (nm, ± 3)[a]	Pattern depth d (nm, ± 2)[a]	t (nm) [b]	Effective index (TE mode)[c]
Film A	$c_{max}/4$	200	22	25	1.569
Film B	$c_{max}/2$	209	38	34	1.577
Film C	c_{max}	253	61	78	1.598

[a]Corresponds to measured data.
[b]Corresponds to deduced data.
[c]Corresponds to c data calculated using the 1-D modesolver software.[13]

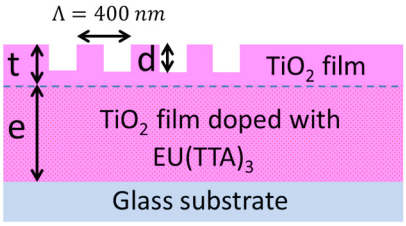

Fig. 2 Scheme of the structure under study.

to be the same for all samples, with a value of 175 nm. This result was confirmed by ellipsometry (MM-16 Horiba Jobin Yvon) measurements. Moreover, AFM provides a precise measurement of the depth of the structure, d. The thicknesses e and $t + e$ of the layer(s) of TiO_2 are measured by scratching the surface after the deposit of one or two layers of TiO_2 and measuring the depth of the scratch by profilometry. For such measurements, an observation under optical microscope is required to make sure the film is cleanly removed and the underneath substrate is not scratched. The results are gathered in Table 1.

2.4 *Optical Characterizations*

The near-normal-incidence extinction is quantified using a Varian Cary 50 Scan UV-visible spectrometer. The light source, provided by a xenon lamp, is focalized on the sample within a spot of about 1 mm^2 and NA ≈ 0.025. All those parameters are set by the commercial apparatus. A measurement is made on a patterned zone and on an unpatterned zone of each sample between $\lambda = 400$ and 800 nm. The apparent absorbance, A_λ, is directly provided by the device. It corresponds to the $\log_{10}$ of the inverse of the transmittance (T_λ) [Eq. (2)]. The transmittance of a clean glass substrate is taken as reference ($T_{\lambda,0}$).

$$A_\lambda = \log_{10}\left(\frac{T_\lambda}{T_{\lambda,0}}\right). \tag{2}$$

3 Results

The efficiency of the PhC is evaluated by studying the apparent absorbance spectra of the different films (Fig. 3), in a patterned (solid line) and in an unpatterned (dashed line) area. For the

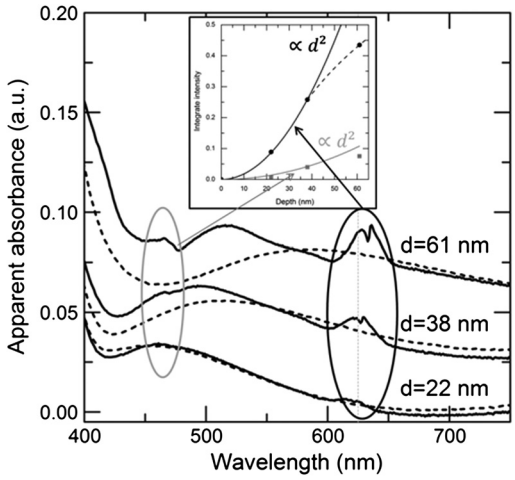

Fig. 3 Apparent absorbance for the three films on a patterned (solid) and nonpatterned zone (dashed). The spectra were artificially shifted for clarity reasons. Vertical line corresponds to $\lambda = 625$ nm. Inset: Area of the massifs at $\lambda = 625$ nm (black) and at $\lambda = 450$ nm (gray) as a function of the pattern depth. For the integration the area between the curve and a straight line joining each side of the peak was considered. At small depth the areas vary proportionally to d^2.

patterned areas, the shape is similar for the three samples: a broad band between 400 and 550 nm and two peaks around 620 nm as predicted [Eq. (1)]. It evidences that, at normal incidence, red light is coupled to the PhC and guided into the film through its two supported modes, TE and TM, associated for instance to the peaks at 621 and 630 nm for $d = 38$ nm. We observe that the deeper the PhC, the stronger the coupling with the external beam. Film C, with $d = 61$ nm, couples the impinging light with the highest efficiency. The integration of the peaks (Inset Fig. 3) provides a more quantitative view of this evolution.

It is interesting to use the strength of the peak to check the predictions of the coupling factor known from Kazarinov theory.[13] The relevant overlap integral intervenes, in this theory [Eqs. (A17)–(A19)], through its square, and thus, the main trend for a given guided mode profile and a layer of variable height with modulated index is a d^2 dependence. By plotting the apparent absorbance area versus pattern depth in inset Fig. 3, we find a good agreement with such a trend for the two first points-films A and B. Film C whose depth of 61 nm is a larger fraction of the wavelength ($\lambda/4n \sim 100$ nm) lies below the extrapolation from films A and B.

Moreover, by subtracting the absorbance measured on unpatterned zones (dashed lines on Fig. 3) an unexpected weak broad band at $\lambda = 450$ nm appears (Fig. 3), which seems to follow the same evolution than one at $\lambda = 620$ nm (see inset). However, at this stage of the exploitation it is impossible to judge if this second group of peaks has physical sense.

Furthermore, a shift of the peak to the higher energies is observed when the effective index decreases: all features shift by $\Delta\lambda \sim +10$ nm from film A to film C, indicating a modification of the guided mode effective refractive index. The effective indices of the TE- and TM-guided modes $n_{\mathrm{effTE,TM}}$ can be calculated using a one-dimensional (1-D) mode solver[13] for the different films considering that the average refractive index for the PhC is $1.6 = 1 * f + 1.79 * (1 - f)$ with an air filling factor $f \sim 0.25$.[6] Results are reported on Table 1. The variations of the effective indices reflect the overall addition of matter that is made when adding the patterned layer. As we deal with deposited matter rather than etching, the deeper pattern in sample C corresponds to the larger amount of deposited matter on the luminescent layer, and thus the higher effective index. The shift observed is therefore consistent with [Eq. (1)], which predicts here a shift of the normal incidence extraction to the longer wavelengths for the higher refractive indices. It means that film C is the most efficient in terms of coupling with the incident light but it will mainly couple light at 630 nm for the near-normal incidence of interest.

In order to go further in the interpretation, 2-D rigorous-coupled wave analysis (RCWA) simulation was performed.[14] First, the aim is to match the experimental curves obtained with the UV-vis spectrometer. In this perspective, we looked at the variations of the zeroth-order transmission as a function of the wavelength, for a fixed incident angle, $\theta = 0$ deg.

Figure 4 shows the result for a structure corresponding to Film C: 200-nm square holes ($n = n_{\mathrm{air}} = 1$) periodically ($a = 400$ nm) distributed in a TiO_2 layer ($n = 1.75$; $d = 61$ nm)

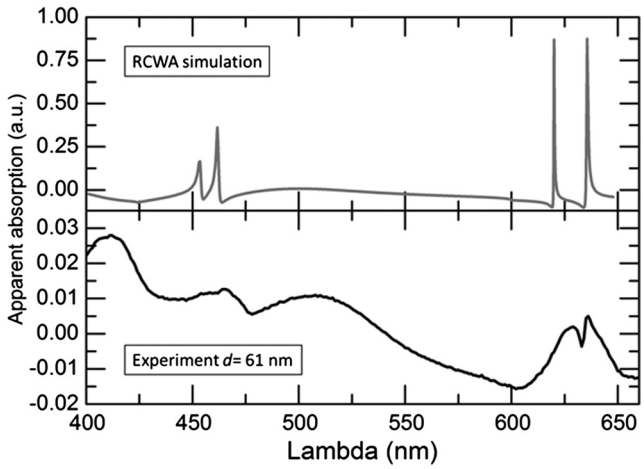

Fig. 4 Apparent absorbance for Film C ($d = 61$ nm) (black) and the corresponding two-dimensional (2-D) rigorous-coupled wave analysis (RCWA) simulations (gray) for an incident angle $\theta = 0$ deg. Note the peaks around 625 and 635 nm correspond to coupling to the guided mode.

on top of a continuous TiO_2 layer ($n = 1.75$) and with a glass substrate ($n = 1.5$). The thickness of each layer can be adjusted to match the experimental sample. The calculation is made for a TM and a TE incident wave, but considering the geometrical symmetries of the system the results are perfectly identical. The simulated curve presents the same two characteristic peaks at 625 and 635 nm as the experimental one. It also shows the two extra peaks at 450 nm, much less intense than those at 625 nm. This proves that the broad band at 450 nm previously described is not an artifact. Moreover, it will be seen later that those peaks disappear in the case of a 1-D simulation. They are thus inherent to the existence of two periodic dimensions in our system.

Furthermore, the simulated peaks are much thinner than the experimental ones and their intensity higher. This can be explained by some of the simplifications taken in the simulations, such as the zero NA (normal incidence) of the incident beam (NA ~ 0.025 in the UV-vis spectrometer used experimentally), its monochromaticity, the perfectly square shape of the patterning.

To investigate the role of the effects mentioned above, we first checked if, by choosing a suitable system, we could reasonably use 1-D RCWA[13] simulations instead of 2-D ones. For this new 1-D system a square geometry was used, alternating $n_{TiO_2} = 1.75$ corresponding to a line full of TiO_2 and an effective index of $n_{mean} = 1.375$ corresponding to a line containing one half of TiO_2 and half air (Fig. 4). As for the 2-D case, the periodic grating is deposited on top of a plain layer of TiO_2 and a glass substrate. The simulation is performed for TE and TM incident waves. The results are gathered in Fig. 5. The adaptation of the system to 1-D involved the loss of symmetry, thus the results are different for a TE and a TM incident wave. Nevertheless, as the spectrometer informs us on diverted light, by combining additively the two polarizations of the 1-D absorption simulation, the two peaks around 625 and 635 nm of the 2-D simulation are perfectly reproduced. Even so, however, the 1-D calculation does not allow reproducing the feature around $\lambda = 450$ nm, as those are related to coupling by 2-D reciprocal wavevectors at 45 deg from photonic crystal axis. Thus, the 1-D model is sufficient to study the effects occurring between 600 and 650 nm and in particular to investigate the impact of the dispersion in angle around the normal incidence on the features of the peaks. Moreover, there is a ten-fold computational speed up between 1-D and 2-D RCWA.

In this context, a system corresponding to the film B was simulated and the incident angle was scanned from $\theta = 0$ to 1.4 deg (thus by symmetry from -1.4 to 1.4 deg), corresponding to the larger angle permitted considering NA = 0.025, and with a step of 0.2 deg. The results are presented in Fig. 6. A split of each peak, increasing when moving away from the normal incidence, is observed. In order to take into account the shape of the incident beam, the following weighting factor was used: $f_\theta = \sqrt{\theta^2_{max} - \theta^2}$. Thus, the angle aperture of the spectrometer

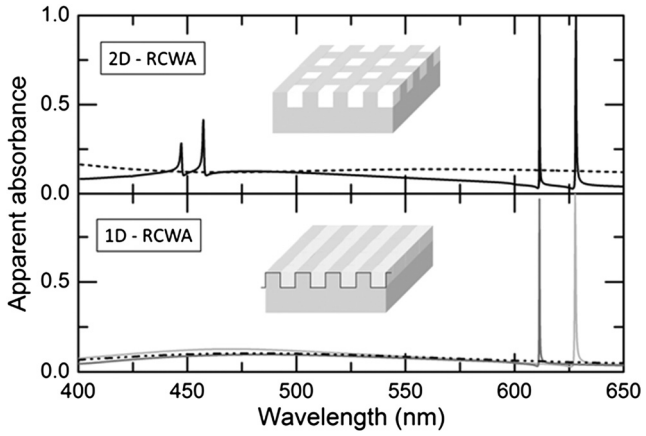

Fig. 5 Comparison of the one-dimensional (1-D) and 2-D RCWA simulations for a system corresponding to film B ($d = 38$ nm). Top graph presents the 2-D calculation for a pattern (solid black curve) and an un-patterned (dashed black curve) zone. Bottom graph presents the 1-D calculation for a patterned zone with a TE (solid gray curve) and a TM (solid dark gray curve) incident wave and an unpatterned zone (dashed black curve). The inserts show a schematic view of the system used for the 2-D and 1-D calculations.

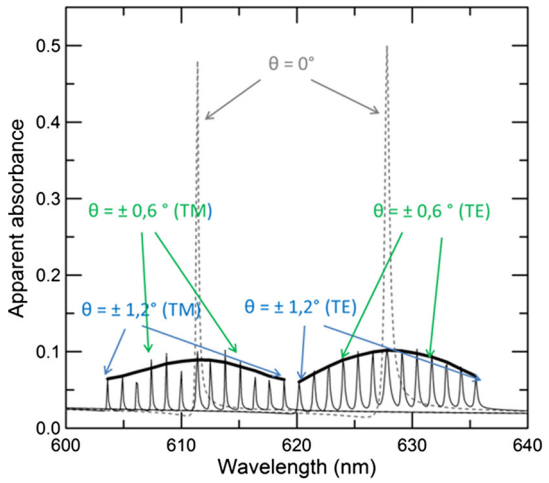

Fig. 6 Explanation of broadening of experimental peaks seen in Fig. 4 for $\lambda = 600:640$ nm. Angle aperture spectrometer has beam divergence of around 1.4 deg.

satisfactorily explains the average and the enlargement of the experimental signal compared with the simulated one, but, as mentioned before, this may not be the only effect.

Second, we attempted to exploit angular spectra for extraction length determination. Still, considering the effective 1-D system, the incident wavelength was fixed at $\lambda = 650$ nm, and we scanned the zeroth-order transmission as a function of the incident angle (Inset Fig. 7). The resonance wavelength previously determined was not considered to avoid side effects present at $\theta = 0$ deg. The simulated system is similar to the previous one, but the pattern depth d is modulated from 10 to 80 nm. The shape of the peak is in agreement with the literature.[15,16] For each depth, the full-width at half maximum (FWHM, $\Delta\theta$) is determined and presented in Table 2. Then, Matioli's method, which relates the extraction length L_{ext} to the width of the diffraction bands, can be applied in this case [Eq. (3)].[7]

$$L_{\text{ext}} = \frac{2}{\Delta k_1} = \frac{2}{k_0 \Delta\theta \cos\theta} = \frac{\lambda^2}{\pi \sin\theta \Delta\lambda}. \tag{3}$$

The extraction lengths (distance that light propagates in the film before being extracted) deduced from the simulations are presented in Fig. 7. The order of magnitude of those values is consistent with the experimental ones presented in the literature.[8]

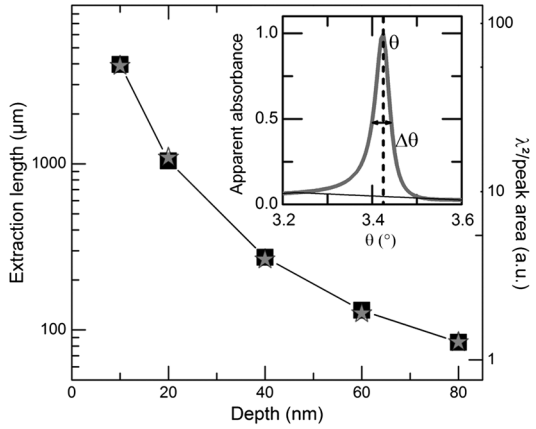

Fig. 7 Evolution of the extraction length (squares) and of λ^2 divided by simulated peak area (star) as a function of pattern depth. The extraction length was calculated from the full-width at half maximum (FWHM) values of the simulated peaks by applying Eq. (3). Inset: (gray) Calculation for the effective 1-D system with $d = 40$ nm and an incident wave at $\lambda = 650$ nm as a function of the incidence angle. (Black) baseline. θ corresponds to the maximum of the peak and $\Delta\theta$ to the FWHM.

Table 2 Simulated full-width at half maximum (FWHM) in milliradians and degrees for different pattern depths, d.

	FWHM	
d (nm)	mrad	(degree)
10	2.56E – 2	(1.41E – 3)
20	1.99E – 1	(1.14E – 2)
40	7.57E – 1	(4.33E – 2)
60	1.58	(9.05E – 2)
80	2.46	(1.4E – 1)

Furthermore, theoretically it is possible to relate as well L_{ext} to $\Delta\lambda$ [Eq. (3)] and then, deduce L_{ext} experimentally, directly from the FWHM of the coupling peak in the apparent absorbance spectra. Nevertheless, the spectra should be taken with an incident angle θ nonequal to zero to avoid the singularity at normal incidence. Moreover, using a UV-visible spectrometer does not provide the required resolution. This direct measurement is thus not applicable in our case. But, we note that the evolutions of L_{ext} and of the inverse peak area as a function of d are similar (Fig. 7); the peak area (if we use the same spectrometer) is an adequate measurement to compare quantitatively the coupling strength.

4 Conclusion

We presented a simple experimental method to measure the efficiency of the PhC. Contrarily to the characterization methods described in the literature; it does not need complex set up, a simple routine UV-vis spectrometer allows to get the essential data to provide a desirable feedback in a quest of an optimum PhC depth for light extraction.

Moreover, we demonstrated both experimentally and numerically, the influence of the pattern depth on the light extraction for a light emitting device comprising a nearly single-mode waveguide. We found a good correspondence between experimental and numerical results.

The coupling first increases proportionally to d^2 as predicted by theory[12] for small modulation depths. It has been shown that extraction length of guided mode is varying between a hundred and a few thousands of wavelengths of incident light. Our combination of numerical approach and use of routine instruments can be used to further optimization of extracting structures and to greatly facilitate experiment design, from preparation to follow-up. For example, it can be apply to study the influence of other parameters on the light extraction such as the hole shape, lattice, and periodicity.

Acknowledgments

L. Devys and G. Dantelle prepared the samples, L. Devys and V. Kubytskyi performed the RCWA simulations, H. Benisty and T. Gacoin initiated and supervised the project. All authors participated to the analysis of the results.

References

1. R. Bathelt et al., "Light extraction from OLEDs for lighting applications through light scattering," *Org. Electron.* **8**(4), 293–299 (2007), http://dx.doi.org/10.1016/j.orgel.2006.11.003.
2. J. J. Shiang, T. J. Faircloth, and A. R. Duggal, "Experimental demonstration of increased organic light emitting device output via volumetric light scattering," *J. Appl. Phys.* **95**, 2889–2895 (2004), http://dx.doi.org/10.1063/1.1644038.

3. D.-S. Liu et al., "Light-extraction enhancement in GaN-based light-emitting diodes using grade-refractive-index amorphous titanium oxide films with porous structures," *App. Phys. Lett.* **94**, 143502 (2009), http://dx.doi.org/10.1063/1.3116613.
4. S. Chen and H. S. Kwok, "Light extraction from organic light-emitting diodes for lighting applications by sand-blasting substrates," *Opt. Express* **18**, 37–42 (2010), http://dx.doi.org/10.1364/OE.18.000037.
5. A. David, H. Benisty, and C. Weisbuch, "Photonic crystal light-emitting sources," *Rep. Prog. Phys.* **75**, 126501 (2012), http://dx.doi.org/10.1088/0034-4885/75/12/126501.
6. A. Revaux et al., "Photonic crystal patterning of luminescent sol-gel films for light extraction," *Nanotechnology* **22**, 365701 (2011), http://dx.doi.org/10.1088/0957-4484/22/36/365701.
7. E. Matioli et al., "Measurement of extraction and absorption parameters in GaN-based photonic-crystal light-emitting diodes," *J. Appl. Phys.* **107**, 053114 (2010), http://dx.doi.org/10.1063/1.3309837.
8. L. Devys et al., "Extraction length determination in patterned luminescent sol-gel films," *Adv. Opt. Mat.* **2**, 81 (2014), http://dx.doi.org/10.1002/adom.201300304.
9. G. A. Turnbull et al., "Relationship between photonic band structure and emission characteristics of a polymer distributed feedback laser," *Phys. Rev. B* **64**, 125122 (2001), http://dx.doi.org/10.1103/PhysRevB.64.125122.
10. G. A. Turnbull et al., "Photonic mode dispersion of a two-dimensional distributed feedback polymer laser," *Phys. Rev. B* **67**, 165107 (2003), http://dx.doi.org/10.1103/PhysRevB.67.165107.
11. C. de Silva et al., "Adducts of europium b-diketonates with nitrogen p,p'-disubstituted bipyridine and phenanthroline ligands: synthesis, structural characterization, and luminescence studies," *Inorg. Chim. Acta* **360**, 3543–3552 (2007), http://dx.doi.org/10.1016/j.ica.2007.04.049.
12. M. J. Hampton et al., "The patterning of sub-500 nm inorganic oxide structures," *Adv. Mater.* **20**, 2667–2673 (2008), http://dx.doi.org/10.1002/adma.v20:14.
13. R. Kazarinov and C. Henry, "Second-order distributed feedback lasers with mode selection provided by first order radiation losses," *IEEE J. Quantum. Electron.* **21**, 144–150 (1985), http://dx.doi.org/10.1109/JQE.1985.1072627.
14. P. Kwiecien, 2D-RCWA, http://sourceforge.net/projects/rcwa-2d/; P. Kwiecien, 1D-RCWA, http://sourceforge.net/projects/rcwa-1d/.
15. S. M. Norton, T. Erdogan, and G. M. Morri, "Coupled-mode theory of resonant-grating filters," *JOSA A* **14**, 629 (1997), http://dx.doi.org/10.1364/JOSAA.14.000629.
16. D. Rosenblatt, A. Sharon, and A. A. Friesem, "Resonant grating waveguide structures," *IEEE J. Quantum Electron.* **33**, 2038 (1997), http://dx.doi.org/10.1109/3.641320.